

1 **Measurements of non-volatile aerosols with a VTDMA and**
2 **their correlations with carbonaceous aerosols in**
3 **Guangzhou, China**

4

5 **H. H. Y. Cheung¹, H. B. Tan², H. B. Xu³, F. Li², C. Wu¹, J. Z. Yu^{1,4} and C. K. Chan^{1,5,6}**

6 [1]{Division of Environment, Hong Kong University of Science and Technology, Hong Kong,
7 China}

8 [2]{Institute of Tropical and Marine Meteorology, China Meteorological Administration,
9 Guangzhou, China}

10 [3]{Sun Yat-sen University, Guangzhou, China}

11 [4]{Department of Chemistry, Hong Kong University of Science and Technology, Hong Kong,
12 China}

13 [5]{Department of Chemical and Biomolecular Engineering, Hong Kong University of Science
14 and Technology, Hong Kong, China}

15 [6]{School of Energy and Environment, City University of Hong Kong, Hong Kong, China}

16 Correspondence to: H. B. Tan (hb tan@gmcc.gov.cn), C. K. Chan (chak.k.chan@cityu.edu.hk)

17

1 **Abstract**

2 Simultaneous measurements of aerosols of varying volatilities and carbonaceous matters were
3 conducted at a suburban site in Guangzhou, China in February and March 2014 using a
4 volatility tandem differential mobility analyzer (VTDMA) and an organic carbon/ elemental
5 carbon (OC/EC) analyzer. Low-volatility (LV) particles, with a volatility shrinkage factor (*VSF*)
6 at 300 °C exceeding 0.9, contributed to 5% of number concentrations of 40 nm particles and
7 11–15% of 80–300 nm particles. They were non-volatile materials externally mixed with the
8 volatile ones and therefore did not evaporate significantly at 300 °C. Non-volatile materials
9 mixed internally with the volatile ones are referred to as the medium volatility (MV, $0.4 < VSF$
10 < 0.9) and high volatility (HV, $VSF < 0.4$) particles. These MV and HV particles contributed to
11 57–71% of number concentrations for particles between 40 nm and 300 nm in size. The average
12 EC and OC concentrations measured by the OC/EC analyzer were $3.4 \pm 3.0 \mu\text{g m}^{-3}$ and $9.0 \pm$
13 $6.0 \mu\text{g m}^{-3}$, respectively. Non-volatile OC evaporating at 475 °C or above, together with EC,
14 contributed to 67% of the total carbon mass. The diurnal variations in the volume fraction of
15 the volatile materials, HV, MV and LV residuals were less than 15% for most of the particles
16 except for the 40 nm ones, although a daily maximum and a daily minimum were still observed.
17 Back trajectory analysis also suggests that over 90% of the air masses influencing the sampling
18 site were well-aged as they were transported at low altitudes (below 1500 m) for over 40 h
19 before arrival. Further comparison with the diurnal variations in the mass fractions of EC and
20 non-volatile OC in $\text{PM}_{2.5}$ suggests that the non-volatile residuals may be related to both EC and
21 non-volatile OC in the afternoon, during which the concentration of aged organics increased.
22 The closure analysis of the total mass of LV and MV residuals and the mass of EC or the sum
23 of EC and non-volatile OC also suggests that non-volatile OC, in addition to EC, was one of
24 the components of the non-volatile residuals measured by the VTDMA in this study.

25

1 **1 Introduction**

2 Carbonaceous aerosols comprising organic carbon (OC) and elemental carbon (EC) or black
3 carbon (BC) are one of the major light absorption constituents and are abundant in particulate
4 matter (PM) (Rosen et al., 1978; Hansen et al., 1984; Japar et al., 1986; Chow et al., 1993;
5 Horvath, 1993; Liousse et al., 1993; Fuller et al., 1999; Putaud et al., 2010; Tao et al., 2014;
6 Zhang et al., 2015). In China, the worsening of visibility degradation associated with PM is of
7 increasing concern in recent years. In particular, numerous studies on air pollution were carried
8 out in different cities in China including the Pearl River Delta (PRD) region which is a fast-
9 developing economic zone (Cheng et al., 2006; Wu et al., 2007; Andreae et al., 2008; Chan and
10 Yao, 2008; Gnauk et al., 2008; Tan et al., 2013a). In 2007, the mass concentrations of EC and
11 OC measured at an urban Guangzhou (GZ) site were reported to be from 6.8 to 9.4 $\mu\text{g m}^{-3}$ and
12 from 13.4 to 22.5 $\mu\text{g m}^{-3}$ respectively (Yu et al., 2010).

13 Soot particles are often characterized in terms of EC and BC, depending on whether they are
14 measured thermally or optically (Penner and Novakov, 1996; Lavanchy et al., 1999; Cheng et
15 al., 2011 and references therein). Their optical properties are distinct when they are freshly
16 produced (Novakov et al., 2003). After aging processes such as cloud processing, reaction with
17 other species and coagulation, their structure, shape, size, mixing state and thus optical
18 properties change (Horvath, 1993; Liousse et al., 1993; Ghazi and Olfert, 2012). EC is typically
19 measured by thermal method such as the OC/EC analyzer (Chow et al., 2007), BC are optically
20 measured using instruments such as aethalometer (Hansen et al., 1984), multi-angle absorption
21 photometer (Petzold and Schönlinner, 2004) and particle soot absorption photometer (Virkkula
22 et al., 2005). However, it is not possible to retrieve the mixing state of soot particles from above
23 techniques. To determine the mixing state of soot particles, single particle soot photometer
24 (Stephens et al., 2003), soot particle aerosol mass spectrometer (Onasch et al., 2012) and
25 Volatility Tandem Differential Mobility Analyzer (VTDMA) (Philippin et al., 2004) have been
26 used.

27 Ambient aerosols have varying volatility properties based on their chemical compositions.
28 VTDMA was first introduced by Rader and McMurry (1986) to study the behavior of aerosols
29 upon thermal treatment. Philippin et al. (2004) later developed a VTDMA which is capable of
30 evaporating volatile materials in aerosols at temperatures up to 300 °C. Non-volatile materials
31 at 300 °C, such as EC, non-volatile organics and sea salt, can internally mix with (or be coated
32 with) volatile materials. Note that the terms “volatile” and “non-volatile” are defined at the

1 heating temperature of 300 °C in the VTDMA. They are different from the volatilities defined
2 under ambient conditions (Donahue et al., 2009; Murphy et al., 2014) or in other measurement
3 techniques (Twomey, 1968; Pinnick et al., 1987; Huffman et al., 2009). The composition of
4 these non-volatile residuals can vary spatially and temporally in VTDMA measurements.
5 Previous studies have demonstrated good agreement between the mass of black carbon and the
6 mass of particles with small volatile fractions, which experienced size reductions of 5 to 10%
7 upon heating at 300 °C in the VTDMA. Various studies have also used an VTDMA to estimate
8 the mixing states of soot particles. Particles with small volatile fractions are often assumed to
9 be soot particles externally mixed with particles with volatile materials at 300 °C. Particles with
10 larger volatile fractions, which experienced size reductions of more than 10% upon heating at
11 300 °C in the VTDMA, were assumed to represent soot particles internally mixed (coated) with
12 the volatile materials (Philippin et al., 2004; Cheng et al., 2006; Frey et al., 2008; Wehner et al.,
13 2009; Rose et al., 2011; Levy et al., 2014; Zhang et al., 2016).

14 Organics also contribute to light absorption by atmospheric particles (Bond, 2001; Kirchstetter
15 et al., 2004; Chen and Bond, 2010). Laboratory studies have shown that organic aerosols may
16 form low volatility oligomers after aging for a long time (e.g. Kalberer et al., 2004). Huffman
17 et al. (2009) showed that highly oxygenated, aged organic aerosols exhibited similar or lower
18 volatility than the primary organic aerosols or the less oxygenated ones. Recently, Häkkinen et
19 al. (2012) found that the mass fraction remaining (MFR) of non-BC residuals, i.e. the difference
20 between the residual mass derived from a volatility differential mobility particle sizer at 280 °C
21 and black carbon mass derived from an aethalometer, is positively correlated with the mass
22 fraction of organics measured by an AMS.

23 In this study, simultaneous measurements of aerosols volatility and carbonaceous matter were
24 made at a suburban site in Guangzhou, China during wintertime in February and March 2014
25 using a VTDMA and a semi-continuous OC/EC analyzer, respectively. Volatility
26 measurements were made for ambient aerosols ranging from 40 nm to 300 nm in diameter.
27 Residuals remaining after heating at 300 °C in the VTDMA are referred to as non-volatile in
28 this study. We report the average values, time series and diurnal variations in the number and
29 volume fractions of the volatile and non-volatile materials, as well as the OC and EC
30 concentrations. We examine the relationships of the non-volatile materials upon heating at
31 300 °C to EC and to the non-volatile OC, based on analyses of the diurnal patterns and mass
32 closures of the OC/EC and VTDMA data. Finally, we discuss the influence of air mass origins

1 on the volatility of the sampled aerosols and concentrations of OC and EC based on back
2 trajectory analysis.

3

4 **2 Methodology**

5 **2.1 Experimental**

6 **2.1.1 Measurement details**

7 The campaign was taken place at the China Meteorological Administration (CMA)
8 Atmospheric Watch Network (CAWNET) Station in Panyu, Guangzhou, China in summer
9 from July to September 2013 and winter from 6 February to 21 March 2014, which is operated
10 by the Institute of Tropical and Marine Meteorology (ITMM) of the CMA. The Panyu station
11 is located at the center of the PRD region and on the top of Dazhengang Mountain (23°00' N,
12 113°21' E) with an altitude of about 150 m (Figure S1 in Supplemental Information) (Tan et al.,
13 2013a). It is about 120 m above the city average elevation and is surrounded by residential
14 neighborhoods with no significant industrial pollution sources nearby. Measurements of
15 particle number size distributions, volatility, mass concentrations of EC and OC were made in
16 winter from 6 Feb to 21 Mar 2014. Some of the measurements were not made continuously due
17 to maintenance work and hence only periods with both VTDMA and OC/EC measurements
18 were analyzed.

19 **2.1.2 VTDMA measurements**

20 We used a custom-made VTDMA based on a Hygroscopic TDMA system developed in ITMM
21 (Tan et al., 2013b), with the humidifier between the two DMAs replaced by a heated tube which
22 effect evaporation of volatile materials. In our VTDMA system shown in Figure 1, ambient
23 aerosols sampled by a PM_{2.5} inlet first passed through a dryer at relative humidity below 20%.
24 The dry aerosols then passed through a neutralizer and entered the first differential mobility
25 analyzer (DMA₁) (Stream 1) to produce mono-disperse aerosols of diameter between 40 nm
26 and 300 nm, D_0 . The mono-disperse aerosols went either path (a) or (b) in Fig. 1 after leaving
27 DMA₁. In path (a), they (Stream 2) were directed to a condensation particle counter (CPC, TSI
28 Model 3772) to obtain particle counts, N_{D_0} . The particle number size distribution of the ambient
29 aerosols, $dN/d\log D_p$, was also measured by varying the DMA₁ voltage (SMPS scan).
30 Afterwards, the mono-disperse aerosols were directed via path (b) to a heated tube for volatility

1 measurement (V-Mode) sequentially at 25 °C, 100 °C and 300 °C. The heating tube was a 1/2",
2 80 cm long stainless steel tube with an inner diameter of 8 mm. With a sample flow rate of 1 L
3 min⁻¹, the resulting residence time in the heated section of the VTDMA was 2.4 s. The estimated
4 aerosol velocity on the center line was 0.33 m s⁻¹. Compared to the residence time of 0.3 s to 1
5 s in other VTDMA systems (e.g. Brooks et al., 2002; Philippin et al., 2004; Villani et al., 2007),
6 the residence time in our VTDMA is assumed to be long enough for the volatile materials to be
7 effectively vaporized. After leaving the heating tube, the flow entered a heat exchanger
8 measuring 30 cm in length to ensure sufficient cooling before entering DMA₂.

9 Upon heating at 100 °C and above, volatile components of particles such as sulfate, nitrate and
10 volatile organics would vaporize at different temperatures depending on their volatilities. A
11 volatility shrinkage factor, *VSF*, is defined as the ratio of particle diameter after heating at
12 temperature *T*, *D_{p,T}*, to that before heating, *D₀*, to indicate the size reduction of the ambient
13 particles (Eq. (1)). The value of *VSF* is always smaller than or equal to one, depending on the
14 amount of volatile materials vaporized at the heating temperature *T*.

$$15 \quad VSF(T) = \frac{D_{p,T}}{D_0} \quad (1)$$

16 The *VSF* is also used to divide the particles into three groups, namely the low volatility (LV),
17 medium volatility (MV) and high volatility (HV) particles. In this study, we focus on the
18 measurements made at 300 °C. The *VSF* ranges for LV, MV and HV particles upon heating at
19 300 °C are above 0.9, between 0.4 and 0.9 and below 0.4, respectively (Fig. 2) (Wehner et al.,
20 2004; Wehner et al., 2009). The LV particles are assumed to represent EC particles externally
21 mixed with the volatile materials, while MV and HV particles are assumed to represent EC
22 particles internally mixed with volatile materials. While the volatile materials in the MV and
23 HV particles are referred to as VM, those exist as external mixtures with the LV, MV and HV
24 particles are referred to as completely vaporized (CV) particles. The CV particles evaporate
25 completely without leaving behind any residuals at 300 °C. Excluding particle diffusional and
26 thermophoretic losses, the evaporation of VM and CV does not change the number
27 concentrations of LV, MV and HV particles.

28 The new size distribution, *dN'/dlogD_p* of the remaining particles (hereafter the residuals) were
29 measured by DMA₂ and CPC before they were heated at another temperature (Fig. 2b). Overall
30 it took around one and a half to two hours to complete a cycle of measurements which consisted
31 of SMPS scans and V-Mode measurements at 25 °C, 100 °C and 300 °C. At each temperature,
32 the sampling time for six selected diameters from DMA₁ (40 nm, 80 nm, 110 nm, 150 nm, 200

1 nm and 300 nm) took about half an hour and SMPS scans were made in-between. Hereafter,
2 notations with the superscript prime refer to the LV, MV or HV residuals measured by DMA₂
3 and CPC after heating, while the corresponding ones without the prime refer to the LV, MV or
4 HV residuals in ambient aerosols prior to heating.

5 **2.1.3 OC/EC measurements**

6 A semi-continuous Sunset OC/EC Analyzer (Model 4) was used to measure PM_{2.5} mass
7 concentrations of organic carbon and elemental carbon, m_{OC} and m_{EC} respectively, on an hourly
8 basis (Turpin et al., 1990; Birch and Cary, 1996; Wu et al., 2012). The OC/EC Analyzer adopts
9 the ACE-Asia protocol (a NIOSH-derived protocol), where OC evaporates at four set
10 temperatures of 310 °C, 475 °C, 615 °C and 870 °C with pure helium (He) as the carrier gas, and
11 EC is combusted at temperatures between 550 °C and 870 °C under He and 2% oxygen (O₂)
12 (Schauer et al., 2003; Wu et al., 2012). The OC contents are named OC₁ to OC₄ based on the
13 temperature protocol of the OC/EC analyzer (Table 1). The mass of EC determined at different
14 temperatures will be grouped together for discussions. In the VTDMA measurements, there
15 were volatile or semi-volatile OC which vaporize at 300 °C or below. These vaporized OC are
16 assumed to be OC₁, which vaporizes at 310 °C, although this OC/EC set temperature is slightly
17 higher than the set temperature of 300 °C in the VTDMA. With this assumption, the residuals
18 of the VTDMA at 300 °C (LV and MV residuals) are postulated to consist of (1) OC₂ to OC₄,
19 which vaporize at 475 °C and above, and (2) EC and other refractory PM components. We have
20 ignored the HV residuals as their contributions to the total volume of the particles are
21 insignificant when compared to LV and MV residuals (Section 3.1). We will conduct a mass
22 closure analysis based on the VTDMA and OC/EC measurements to examine this assumption.

23 **2.2 Data analysis**

24 **2.2.1 Number fractions**

25 The number fractions of LV, MV and HV residuals ($\Phi'_{N,LV}$, $\Phi'_{N,MV}$ and $\Phi'_{N,HV}$, with their sum
26 being equal to unity) in Stream 2 on Fig. 1 were obtained from $dN'/d\log D_p$ measured by the
27 CPC. However, these fractions do not represent the actual number fractions of LV, MV and HV
28 particles ($\Phi_{N,LV}$, $\Phi_{N,MV}$ and $\Phi_{N,HV}$) before heating because they have not taken into account the
29 CV particles and particle diffusional and thermophoretic losses. The number fraction of CV

1 ($\Phi_{N,CV}$) is first obtained by considering the number fractions due to the residuals ($1-\Phi_{N,CV}$) and
 2 the number concentrations at a selected diameter D_0 before heating (N_{D_0}) and after heating (N'):

$$3 \quad N_{D_0} \times \eta_{D_0} \times (1 - \Phi_{N,CV}) = N' \quad (2)$$

4 where η_{D_0} is the transport efficiency of particles.

5 Equation (2) assumes that η is the same for LV, MV and HV particles. η accounts for particle
 6 loss between DMA₁ and DMA₂ due to diffusion and thermophoretic forces (Philippin et al.,
 7 2004), and it varies with particle size and heating temperature. η at each particle diameter and
 8 VTDMA temperature was determined by laboratory calibrations with sodium chloride (NaCl)
 9 particles, which do not evaporate (i.e., $\Phi_{N,CV} = 0$) at the temperatures used in our experiments.
 10 The transmission efficiency of NaCl of several selected diameters heated at temperatures
 11 between 50 °C and 300 °C is provided in the supplemental information (Fig. S2). From the
 12 known η and field measurements N_{D_0} and N' , $\Phi_{N,CV}$ was obtained from Eq. (2). Afterwards,
 13 $\Phi'_{N,LV}$, $\Phi'_{N,MV}$ and $\Phi'_{N,HV}$ were obtained by renormalizing $\Phi'_{N,LV}$, $\Phi'_{N,MV}$ and $\Phi'_{N,HV}$ with $(1-\Phi_{N,CV})$
 14 so that the sum of $\Phi_{N,LV}$, $\Phi_{N,MV}$, $\Phi_{N,HV}$ and $\Phi_{N,CV}$ equals to unity.

15 **2.2.2 Volume fractions**

16 The volume fractions of LV, MV, HV residuals and CV ($\Phi_{V,LV}$, $\Phi_{V,MV}$, $\Phi_{V,HV}$ and $\Phi_{V,CV}$) at each
 17 selected diameter D_0 are defined as the ratios of the volume of LV, MV, HV residuals and CV
 18 to the total volume of the mono-disperse particles before heating. By assuming that the residuals
 19 are in spherical shape, $\Phi_{V,LV}$, $\Phi_{V,MV}$ and $\Phi_{V,HV}$ can be calculated by:

$$20 \quad \Phi_{V,i} = \frac{N_i \times \frac{\pi}{6} D_{p,i}^3}{N_{D_0} \times \frac{\pi}{6} D_0^3} = \Phi_{N,i} \times \frac{D_{p,i}^3}{D_0^3} \quad (3)$$

21 where N_i and $D_{p,i}$ are the number concentration and mean residual diameter of $i = LV, MV$ or
 22 HV residuals.

23 For LV particles, it is assumed that D_0 and mean D_p are the same and hence $\Phi_{V,LV}$ is the same
 24 as $\Phi_{N,LV}$. For MV and HV particles, the mean D_p is smaller than D_0 due to the evaporation of
 25 volatile materials. The number weighted mean residual diameter (D_p) is calculated by:

$$26 \quad D_{p,i} = \frac{\sum_j D_{p,i} \times N_{i,j}}{N_i} \quad (4)$$

27 where $D_{p,i}$ and $N_{i,j}$ are the residual diameter and number concentration of $i = MV$ or HV at the
 28 75 diameter bins (j) of VSF, respectively.

1

2 The volume fractions of the evaporated materials are calculated from the volume fractions of
3 the residuals. The calculation for $\Phi_{V,CV}$ is similar to that for $\Phi_{V,LV}$. Since the particle has
4 completely vaporized, the vaporized volume is equivalent to the volume of the original particle.
5 Hence, $\Phi_{V,CV}$ is the same as $\Phi_{N,CV}$:

$$6 \quad \Phi_{V,CV} = \frac{N_{CV} \times \frac{\pi}{6} D_{p,CV}^3}{N_{D0} \times \frac{\pi}{6} D_0^3} = \Phi_{N,CV} \quad (5)$$

7 where $D_{p,CV} = D_0$. Since the sum of the total volume fraction of CV, VM and the residuals of
8 LV, MV, HV equals to unity, $\Phi_{V,VM}$ was obtained after the above volume fractions were
9 calculated. Furthermore, we also calculated the volume fraction remaining (*VFR*), defined as
10 the volume ratio of the residual to its host particle, to aid our discussions later:

$$11 \quad VFR_i = \frac{N_i \times \frac{\pi}{6} D_{p,i}^3}{N_i \times \frac{\pi}{6} D_0^3} = \frac{D_{p,i}^3}{D_0^3} \quad (6)$$

12 where N_i and $D_{p,i}$ are the number concentration and mean residual diameter of $i = MV$ or HV
13 after heating, respectively.

14 **2.2.3 Particle size distributions of number, volume and mass concentrations of** 15 **LV, MV and HV residuals**

16 Due to the differences in the size cuts of the VTDMA and the OC/EC Analyzer, log-normal fits
17 extrapolated to 5 μm were applied to the particle number size distributions of the residuals of
18 LV, MV and HV ($dN/d\log D_{p,i}$, where $i = LV, MV$ or HV) to estimate the volume and then mass
19 concentrations (calculated later) of the ambient aerosols for comparison with $\text{PM}_{2.5}$ OC/EC
20 measurements. The volume size distributions ($dV/d\log D_{p,i}$) are calculated by:

$$21 \quad \frac{dV}{d\log D_{p,i}} = \frac{dN}{d\log D_{p,i}} \times \frac{\pi}{6} D_{p,i}^3 \quad (7)$$

22 where $D_{p,i}$ is the mean residual diameter as defined in Section 2.2.2.

23 Volume (V) concentrations of LV, MV and HV residuals can then be calculated by integrating
24 the area under the fitted curves. As we only focus on LV and MV, densities of 1.0 g cm^{-3}
25 (Hitzenberger et al., 1999) and 1.5 g cm^{-3} are applied to V_{LV} and V_{MV} to obtain mass (m)
26 concentrations of LV and MV residuals, respectively. The choice of the densities is based on
27 the assumption that LV and MV residuals are dominated by soot and non-volatile OC,
28 respectively.

1 **3 Results and Discussions**

2 **3.1 Overview**

3 The time series of meteorological conditions, particle number size distribution, PM_{2.5}, OC and
4 EC concentrations during the campaign are presented in Fig. 3. Overall, the campaign came
5 under the influence of the prevailing northerly wind with an average wind speed and
6 temperature (\pm one standard deviation) of $1.73 \pm 0.95 \text{ m s}^{-1}$ and $14.8 \pm 5.1 \text{ }^\circ\text{C}$, respectively. The
7 average PM_{2.5} concentration was $48 \pm 26 \text{ } \mu\text{g m}^{-3}$. A few cold front periods were observed,
8 during which the wind speed increased and the temperature decreased. In general, the low wind
9 speed favored the accumulation of PM_{2.5}. OC concentrations ranged from 0.5 to $47.0 \text{ } \mu\text{g m}^{-3}$
10 with an average of $9.0 \pm 6.0 \text{ } \mu\text{g m}^{-3}$, while EC concentrations ranged from 0.2 to $23.0 \text{ } \mu\text{g m}^{-3}$
11 with an average of $3.4 \pm 3.0 \text{ } \mu\text{g m}^{-3}$. OC₁, the most volatile group among OC₁ to OC₄ in OC/EC
12 analysis, accounted for one-third of the total carbon mass (Fig. 4).

13 On Feb 17, and Mar 12 and 17, the daily-averaged PM_{2.5} concentrations exceeded $95 \text{ } \mu\text{g m}^{-3}$;
14 they were nearly twice the daily-averaged values on other days (Fig. 3, shaded area in grey).
15 Results of 72 h back trajectories (Stein et al., 2015; Rolph, 2016) showed that air masses
16 arriving at the site on or before these three days mostly originated from the continental or
17 oceanic area close to Eastern China (Fig. S3). The SMPS data also showed a mode near 100
18 nm with a high particle number concentration (Fig. 3).

19 The temporal variation of the number concentration of MV particles having an initial diameter
20 of 80 nm or above tracked reasonably well with the accumulation of PM_{2.5} as particles aged and
21 became more internally mixed (Fig. 3 and S4). Furthermore, a size dependence was observed
22 for 80 nm to 300 nm MV particles. There were days, e.g., from Feb 24 to Mar 10, when the
23 number concentration of 300 nm MV particles did not track well with PM_{2.5}. The mode of total
24 particle number size distribution was below 100 nm and the number concentrations of 300 nm
25 particles were low (Fig. 3). PM_{2.5} tracked better with the number concentrations of 80 nm to
26 150 nm MV particles (Fig. 4a to S4c) than those of 200 nm and 300 nm MV particles (Fig. S4d
27 and S4e).

28 The average number and volume fractions of CV, HV, MV and LV in VTDMA measurements
29 at 300 °C are summarized in Table 2. VM is internally mixed with (or coated on) MV and HV
30 residuals, and hence does not have a separate contribution to number concentrations. Overall,
31 HV and MV particles, indicator for aged aerosols with internally mixed non-volatile and

1 volatile materials, accounted for 57% to 71% of the total particle number concentration. Non-
2 volatile materials (LV, MV and HV residuals) accounted for 15% to 26% of the total volume
3 of selected particles before heating. While the CV and HV fractions were larger in the finest
4 particles selected ($D_0 = 40$ nm), MV and LV were more abundant in larger particles ($D_0 > 80$
5 nm). As in Rose et al. (2006), fresh emissions like soot adsorbed or absorbed volatile materials
6 during atmospheric processing. Smaller particles grew to a greater extent than the larger ones
7 because of their higher ratios of surface area to volume. When they were heated in the VTDMA
8 at 300 °C, these smaller particles reduced more substantially in size, as reflected in the higher
9 CV and HV fractions and lower MV and LV fractions. The higher abundance of MV and LV
10 in larger size particles could also be explained by the non-volatile primary particles. Yu et al.
11 (2010) reported that the condensation and droplet modes of EC and OC in urban sites of
12 Guangzhou were approximately 400 nm and 900 nm, respectively. The mode of fresh EC
13 emitted from vehicles is also approximately 400 nm (Huang et al., 2006). Larger particles also
14 likely contain more internally mixed aged aerosols (secondary pollutants) than the smaller ones.
15 Nevertheless, the detection limit of the downstream DMA and CPC in the VTDMA system is
16 10 nm. It was assumed that the residuals having a diameter below 10 nm were small enough to
17 be considered as completely vaporized. However, such assumption would lead to an
18 overestimation of CV and an underestimation of the non-volatile residuals for the finest
19 particles selected (with an initial diameter of 40 nm).

20 **3.2 Diurnal variations**

21 Figure 5 shows the diurnal variation of the fraction of CV, HV residual, MV residual, LV
22 residual and VM in the total volume of particles of dry initial diameters of 40, 150 and 300 nm.
23 For 40 nm particles, clear maximum and minimum of the fraction of CV, VM and HV residuals
24 are observed at 08:00 and 13:00, respectively. The diurnal variation of the HV and MV particles
25 in 40 nm particles was clearer in terms of number fraction (Fig. S5). Furthermore, the trend of
26 CV is opposite to those of VM, HV and MV. The increase of CV in 40 nm particles and to a
27 lesser extent of LV in 150 nm and 300 nm particles in the morning is consistent with traffic
28 pattern, where freshly emitted volatile and non-volatile materials, likely OC and EC, are
29 externally mixed and contributed to CV and LV, respectively. As time progresses in a day, the
30 highly volatile species (CV) which were freshly emitted in the morning, may evaporate and
31 react to form less volatile particles and become VM instead of CV (Robinson et al., 2007).
32 Alternatively, these CV particles could also coagulate with smaller particles to form VM

1 containing particles. Less fresh emissions with more CV particles turning into VM on MV and
2 HV particles can explain the trend that the number and volume fractions of CV decreased while
3 those of MV and HV increased (Fig. 5 and Fig. S5).

4 We also used the diurnal variations in the volume fraction remaining (*VFR*), again defined as
5 the volume ratio of the residual to its *host* particle (not to the total volume of all particles), to
6 examine the size changes of the non-volatile residuals of HV and MV particles. The *VFR* of
7 HV did not exhibit any obvious diurnal variations but the *VFR* of MV peaked near 18:00. The
8 *VFR* of 40 nm MV particles increased after 14:00 while those of 150 nm and 300 nm MV
9 particles increased after 15:00. Since the *VFR* of HV and MV were relatively constant during
10 the day, the increase in VM fraction after the morning rush hours is likely attributed to the
11 increase in number concentrations of HV and MV particles instead of changes in the amount of
12 VM on the MV or HV residuals.

13 The diurnal variations for particles larger than 80 nm were much less obvious than those for 40
14 nm particles in this study and in others (Rose et al., 2011; Cheng et al., 2012; Zhang et al.,
15 2016). In winter, the atmosphere is more stable, resulting in a poorer dilution of aged particles
16 with the less polluted aerosols from higher up (Rose et al., 2006). When the aged pollutants
17 were trapped near the ground surface, the effect of aging of fresh emissions weakened.
18 Therefore, although a daily maximum and a daily minimum were still observed for particles
19 larger than 80 nm, the variation was mostly within 15%.

20 The diurnal variations in the mass fractions of OC and EC in PM_{2.5} provided further insights to
21 the observations above (Fig. 6). The OC and EC data on Mar 12 and 17 were excluded since
22 they were more than two standard deviations higher than those on other days. Subtle morning
23 peaks between 06:00 and 10:00 were observed for the volume fraction of LV residuals (Fig. 5).
24 A similar peak was observed for the mass fraction of EC in PM_{2.5} in the morning (Fig. 6). This
25 suggests that LV particles may be related to the EC from vehicle emissions in the morning. This
26 EC was relatively less aged and externally mixed with other volatile materials. In the late
27 afternoon, LV residuals showed another peak between 17:00 and 19:00 whereas the mass
28 fraction of EC in PM_{2.5} exhibited a minimum at 15:00, after which it increased continuously.
29 The continuous increase in EC at night is likely related to the increase of heavy-duty diesel
30 vehicles (Zhang et al., 2015), which was restricted during daytime (Bradsher, 2007).

31 Although OC₁ contributed to about half of the total OC mass, the diurnal variation in the mass
32 fraction of OC in PM_{2.5} was driven by the total mass of OC₂, OC₃ and OC₄ (OC₂₋₄), which

1 reached a minimum between 05:00 and 09:00 and increased until 19:00. OC can be attributed
2 to both primary and secondary sources. The increased mass fraction of OC in PM_{2.5} and OC-
3 to-EC ratio in the afternoon suggest that the sources of OC were less related to traffic but more
4 to the aging and formation of secondary organic aerosols (Turpin et al., 1990; Chow et al.,
5 1996). These OC₂, OC₃ and OC₄ may be highly oxygenated species or oligomers that are less
6 volatile than primary or less oxygenated organics (Kalberer et al., 2004; Huffman et al., 2009).
7 It is interesting to note that the volume fraction of LV residuals and the *VFR* of MV particles at
8 different sizes showed a dip in the afternoon (Fig. 5, third column from the left). The *VFR* of
9 40 nm MV particles showed a dip at 14:00 while those in 150 nm and 300 nm particles showed
10 a dip at 15:00. The volume fraction of LV residuals in 150 nm and 300 nm particles reached a
11 minimum at 13:00 and 15:00, respectively. Because EC decreased between 12:00 and 15:00,
12 the increase in the volume fraction of LV residuals in 150 nm particles since 13:00 and the *VFR*
13 of 40 nm MV particles since 14:00 may be related to the increased presence of aged organics
14 as well as the EC particles which aged via coagulation and condensation.

15 **3.3 Back trajectory analyses**

16 We calculated the 72 h back trajectories of the air masses arriving at the sampling site (23°00
17 N, 113°25' E) at 4 h intervals (at 00:00, 04:00, 08:00, 12:00, 16:00 and 20:00 local time, UTC
18 +8) using the PC version of the HYSPLIT4 (Hybrid Single Particle Lagrangian Integrated
19 Trajectory, version 4) model (Stein et al., 2015; Rolph, 2016). Archived meteorological data
20 from the Global Data Assimilation System (GDAS) 1-deg was employed and the receptor
21 height was set at 500 m above ground level (a.g.l.). The 191 back trajectories calculated were
22 grouped into six clusters based on their spatial distribution (Fig. 7).

23 Overall, the sampling site was mostly affected by northwesterly and northeasterly air masses.
24 Cluster 1 and 3 are coastal and continental air masses, respectively, although both originated
25 from the northeast. Clusters 4, 5 and 6 represent continental air masses originating from the
26 northwest. Cluster 2 is a group of maritime air masses originating from the East China Sea
27 northeast or east of Guangzhou. While air masses in cluster 6 were transported at relatively high
28 speeds and altitudes (over 3000 m a.g.l.), air masses in all the other clusters were transported at
29 an altitude below 1500 m a.g.l. for over 40 h before arriving at the site. Nevertheless, air masses
30 in cluster 6 only persisted for less than three days. Since the corresponding VTDMA and OC/EC
31 data were sometimes unavailable, cluster 6 will be excluded from the following discussion.

1 The average PM_{2.5}, OC and EC concentrations associated with air masses from the northeast of
2 Guangzhou (clusters 1, 2 and 3) were higher than those from the northwest (clusters 4 and 5,
3 Table 3). Days associated with coastal and maritime air masses were more polluted than days
4 associated with continental air masses for several reasons. First, south China as a region is often
5 affected by the high pressure system moving eastward or southward from the continent out to
6 sea in winter. When the maritime or coastal air streams entered from the southeast of the
7 sampling site at Panyu, the atmosphere at the sampling site became more stable with low local
8 wind speeds (e.g. the polluted days on Feb 17 and Mar 12, 16 and 17, Fig. 3 and S3). Local
9 pollutants accumulated and the city was also affected by pollutants from the southeastern areas
10 of the site (e.g. Shenzhen, Nansha and Dongguan). Second, land-sea breeze cycles were
11 observed when the sampling site was under the influence of maritime air masses from Mar 18
12 to 20. During the day, southeasterly wind prevailed and the wind speed was higher. In the
13 evening, the southeasterly wind was gradually replaced by a southwesterly or northwesterly
14 wind and the wind speed decreased (Fig. 3). The cycle started again in the morning when the
15 westerly wind was gradually replaced by southeasterly wind. Such land-sea breeze effects can
16 result in an effective redistribution and accumulation of air pollutants within the PRD region
17 (Lo et al., 2006).

18 Furthermore, PM_{2.5} in the northeastern parts of China can exceed 200 µg m⁻³ due to both
19 enhanced emissions from coal combustion for heating and poor dispersion during wintertime
20 (Gu et al., 2014). Under the influence of the prevailing northerly or northeasterly wind in China,
21 these pollutants were often transported to southern China and the East China Sea (Chen et al.,
22 2012). Pollutants might also have accumulated when the maritime air masses spent about two
23 days across Taiwan and the coast of south China. In contrast, continental air masses in cluster
24 5 moved slightly faster, and were often associated with the cold front period during which the
25 local wind speed and pressure increased but the temperature decreased (Fig. 3). As the cold air
26 masses passed through the city, dispersion and clearance of pollutants were promoted, resulting
27 in lower PM_{2.5} concentrations (Tan et al., 2013a). Therefore, unlike in other coastal cities like
28 Hong Kong (Lee et al., 2013), in Panyu maritime air masses could lead to more severe pollution
29 than the continental ones in winter.

30 The five clusters were further analyzed to study the influence of air mass history on aerosol
31 volatility. The number fractions of CV, HV, MV and LV of the six selected diameters in
32 VTDMA measurements are regrouped based on the clusters as shown in Fig. 8. The total

1 number fractions of the non-volatile residuals (sum of HV, MV and LV) were similar in all
2 clusters. Maritime air masses (cluster 2) had a slightly higher fraction of LV particles while
3 continental air masses originating from the northwest of the site (clusters 4 and 5) had a higher
4 fraction of HV particles. Although the air masses in clusters 1 and 5 originated from farther
5 away and traveled at relatively higher speeds than those in clusters 2, 3 and 4, all clusters
6 involved transport at low altitudes (below 1500 m) for over 40 h, likely due to the generally
7 lower mixing heights in winter. Therefore, aerosols in these air masses were all well-aged upon
8 arrival (Wehner et al., 2009). This could be another reason for the lack of size dependence of
9 the number, volume fractions and diurnal variation for particles larger than 80 nm. When the
10 transported air masses mixed with local pollutants, the size dependence of the number fractions
11 of different volatility groups as well as the aging of local emissions was further reduced.

12 We also examine at the volatility shrinkage factor (*VSF*) distributions of 40 nm, 110 nm and
13 300 nm particles upon heating at 300 °C (Fig. 9). Log-normal fittings with a three-peak solution
14 were applied to the distributions. The average *VSF* modes of the peaks were located at $0.38 \pm$
15 0.021 (peak 1), 0.60 ± 0.066 (peak 2) and 0.95 ± 0.007 (peak 3), respectively. The standard
16 deviation of the corresponding normal distribution (σ) of peak 3 was the smallest among the
17 three peaks ($\sigma < 0.1$). For the same particle size, the *VSF* distributions in the *VSF* range between
18 0.3 and 0.8 in cluster 5 was relatively more uni-modal than those of other clusters (Fig. 9b and
19 9c). This suggests that the composition in cluster 5 was more homogeneous. Cluster 1 also
20 consisted of long-range transported air masses but they likely passed through areas that are
21 more polluted and mixed with different types of pollutants. Note that the fractions of HV, MV
22 and LV have been traditionally defined based on the values of *VSF*, i.e. $HV < 0.4$; $0.4 < MV <$
23 0.9 ; $LV > 0.9$ (Wehner et al., 2009). The *VSF* distributions above suggest that these definitions
24 using $VSF = 0.4$ and 0.9 may need to be re-visited in the future.

25 **3.4 New particle formation**

26 Two new particle formation (NPF) events were observed in the campaign on Feb 20 and Mar
27 13 (Fig. 3). Since VTDMA data were not available during the NPF event on Mar 13, we only
28 focus on the NPF event on Feb 20 which happened after a cold front under a low $PM_{2.5}$
29 concentration. On Feb 20, a sub-20 nm particle mode was first observed at 12:00. This particle
30 mode grew continuously until it reached 120 nm at 02:00 on Feb 21. In VTDMA measurements,
31 a sharp increase in the number concentration of HV particles having an initial diameter of 40
32 nm was observed at 17:00 on Feb 20 (Fig. 10). This event is likely related to the growth of the

1 newly formed particles when they mixed with the volatile materials via condensation or
2 adsorption. As these particles aged further, they grew larger as reflected in the increase in
3 number concentrations of larger MV particles and the increase in PM_{2.5} mass (Fig. 10). The
4 growth of the newly formed particles can also be observed from the number size distributions
5 of HV, MV and LV particles at different times on Feb 20 and 21 (Fig. 11). The mode of HV
6 particles increased from 40 nm at 17:00 to 80 nm at 21:00 on Feb 20 Feb. The mode stayed at
7 80 nm while the corresponding number concentration decreased at 02:00 on Feb 21 Feb. In
8 contrast, the number concentrations of MV particles grew continuously. The HV and MV
9 particle concentrations and diameter modes underwent much smaller changes on the non-event
10 day of Feb 28 (Fig. 11).

11 **3.5 Closure analysis for LV and MV residuals at 300°C, OC and EC**

12 Closure analysis of EC or the sum of EC, OC₂, OC₃, and OC₄ and the total mass of LV and MV
13 residuals is conducted (Fig. 12). Good correlations ($R^2 > 0.9$) for both EC and the sum of EC,
14 OC₂, OC₃, and OC₄ with the total mass of LV and MV residuals were obtained. Nonetheless,
15 the slope for the total mass of LV and MV residuals to the mass of EC (2.94) is more than two
16 times of that for the total mass of LV and MV residuals to the sum of EC, OC₂, OC₃, and OC₄
17 (1.22), indicating that EC alone cannot account for the total mass of LV and MV residuals.
18 Including non-volatile OC (sum of OC₂ to OC₄) give better mass closure with the total of LV
19 and MV residuals. This further supports our initial postulation that the non-volatile residuals
20 which remained intact upon heating at 300 °C in the VTDMA may contain a significant amount
21 of non-volatile OC. However, the total mass of EC, OC₂, OC₃, and OC₄ do not explain all the
22 mass of LV and MV residuals. A possible explanation could be that the vaporizing temperatures
23 of some OC₁ are close to the upper limit (310 °C), hence they were not completely vaporized in
24 the heated tube and remained in non-volatile residuals. The presence of other refractory
25 materials and the assumption made about the density of LV and MV are two other possible
26 explanations.

27 Other possible errors for the closure could be related to the different heating environments in
28 the VTDMA and the OC/EC analyzer. In the OC/EC analyzer, OC was measured when the
29 samples were heated in the presence of a non-oxidative carrier gas (He). In the VTDMA,
30 aerosols were heated in air which contained O₂. Therefore, some “OC₂₋₄” that evaporated at
31 475 °C or above in the OC/EC analyzer may have been oxidized at 300 °C in the VTDMA.
32 Charring of organic matter could also occur (Philippin et al., 2004). Further study is needed to

1 quantify the effect of oxygen on the oxidation of OC in the VTDMA. The extrapolated
2 lognormal fitting of the size distribution of non-volatile particles can also cause errors if the
3 mode diameter of the fitting is beyond the VTDMA's range of measurements. While the
4 VTDMA measured the size distribution of particles between 10 nm and 400 nm in diameter,
5 the OC/EC analyzer took into account particles up to 2.5 μm in diameter. Yu et al. (2010)
6 reported three EC and OC modes between 0.4 μm and 10 μm in ambient aerosols in Guangzhou:
7 0.4, 0.9 and 5 μm . The 0.4 μm mode accounted for 44% to 49% of the measured EC but only
8 17% to 20% of the measured OC.

9

10 **4 Conclusions**

11 This study presents the first VTDMA measurements in a suburban area of Guangzhou in the
12 Pearl River Delta, China during wintertime. The LV fraction was assumed to be EC particles.
13 These particles were externally mixed with volatile materials at 300 $^{\circ}\text{C}$ and contributed to less
14 than 20% of the total particle number concentration at the sampling site. The diurnal variations
15 in the number and volume fractions of LV, MV and HV were much less obvious in this study
16 than in other studies likely because of the more stable atmosphere and poorer dilution of aged
17 aerosols in winter. Back trajectory analysis showed that the measured $\text{PM}_{2.5}$, EC and OC
18 concentrations were higher when the sampling site came under the influence of maritime and
19 coastal air masses originating from the east or northeast of the site. These observations are
20 attributed to the high pressure system on the continent, the prevailing northerly wind and the
21 enhanced pollution from north China in winter. Long-range transport continental trajectories
22 were often associated with the cold front periods during which the dispersion of pollutants was
23 promoted. The number fractions of LV, MV and HV particles did not show much variations
24 among the clusters, likely because the air masses in all clusters were transported at low altitudes
25 (below 1500 m) for over 40 h. They were therefore well-aged upon arrival at the site.

26 While previous studies have demonstrated soot as a major component of the non-volatile
27 residuals at 300 $^{\circ}\text{C}$ measured by the VTDMA, this work identified non-volatile organics as
28 another possible component. The diurnal variations in the LV fractions and the size of the MV
29 residuals may be related to the variation in the abundance of both EC and non-volatile OC,
30 which evaporated at 475 $^{\circ}\text{C}$ and above in the OC/EC analyzer. Analyses of the diurnal variations
31 in the LV fractions and the *VFR* of MV particles, the latter of which reflects the change in size
32 of the non-volatile materials in the MV particles, suggest that the increase in non-volatile

1 fractions and size in the early afternoon may be related to the increase in non-volatile OC in
2 addition to the effects of EC coagulation and condensation. The mass closure analysis of EC
3 and non-volatile OC and the total mass of LV and MV residuals also suggest that non-volatile
4 OC may have contributed to non-volatile residuals in our VTDMA measurements.

5

6

7

8 **Acknowledgements**

9 This work is supported by the Research Grants Council of the Hong Kong Special
10 Administrative Region, China (Project No. 600413), the Natural Science Foundation of China
11 (Grant 41375156), Special Research and Development Fund for Research Institutes
12 (2014EG137243) and the National Key Project of Basic Research (2011CB403403).

13

14

1 **References**

- 2 Andreae, M. O., Schmid, O., Yang, H., Chand, D., Zhen Yu, J., Zeng, L.-M., and Zhang, Y.-
3 H.: Optical properties and chemical composition of the atmospheric aerosol in urban
4 Guangzhou, China, *Atmos. Environ.*, 42, 6335-6350,
5 <http://dx.doi.org/10.1016/j.atmosenv.2008.01.030>, 2008.
- 6 Birch, M. E., and Cary, R. A.: Elemental carbon-based method for monitoring occupational
7 exposures to particulate diesel exhaust, *Aerosol Science and Technology*, 25, 221-241,
8 10.1080/02786829608965393, 1996.
- 9 Bond, T. C.: Spectral dependence of visible light absorption by carbonaceous particles emitted
10 from coal combustion, *Geophysical Research Letters*, 28, 4075-4078,
11 10.1029/2001GL013652, 2001.
- 12 Bradsher, K.: Trucks power China's economy, at a suffocating cost., *The New York Times*, NY,
13 USA, <http://www.nytimes.com/2007/12/08/world/asia/08trucks.html>, 2007.
- 14 Brooks, B. J., Smith, M. H., Hill, M. K., and O'Dowd, C. D.: Size-differentiated volatility
15 analysis of internally mixed laboratory-generated aerosol, *Journal of Aerosol Science*, 33,
16 555-579, [http://dx.doi.org/10.1016/S0021-8502\(01\)00192-6](http://dx.doi.org/10.1016/S0021-8502(01)00192-6), 2002.
- 17 Chan, C. K., and Yao, X.: Air pollution in mega cities in China, *Atmos. Environ.*, 42, 1-42,
18 10.1016/j.atmosenv.2007.09.003, 2008.
- 19 Chen, B., Du, K., Wang, Y., Chen, J., Zhao, J., Wang, K., Zhang, F., and Xu, L.: Emission and
20 transport of carbonaceous aerosols in urbanized coastal areas in China, 2012.
- 21 Chen, Y., and Bond, T. C.: Light absorption by organic carbon from wood combustion, *Atmos.*
22 *Chem. Phys.*, 10, 1773-1787, 10.5194/acp-10-1773-2010, 2010.
- 23 Cheng, Y., He, K.-b., Duan, F.-k., Zheng, M., Du, Z.-y., Ma, Y.-l., and Tan, J.-h.: Ambient
24 organic carbon to elemental carbon ratios: Influences of the measurement methods and
25 implications, *Atmos. Environ.*, 45, 2060-2066,
26 <http://dx.doi.org/10.1016/j.atmosenv.2011.01.064>, 2011.
- 27 Cheng, Y. F., Eichler, H., Wiedensohler, A., Heintzenberg, J., Zhang, Y. H., Hu, M., Herrmann,
28 H., Zeng, L. M., Liu, S., Gnauk, T., Brüggemann, E., and He, L. Y.: Mixing state of
29 elemental carbon and non-light-absorbing aerosol components derived from in situ particle
30 optical properties at Xinken in Pearl River Delta of China, *Journal of Geophysical Research:*
31 *Atmospheres*, 111, D20204, 10.1029/2005JD006929, 2006.
- 32 Cheng, Y. F., Berghof, M., Garland, R. M., Wiedensohler, A., Wehner, B., Müller, T., Su, H.,
33 Zhang, Y. H., Achtert, P., Nowak, A., Pöschl, U., Zhu, T., Hu, M., and Zeng, L. M.:
34 Influence of soot mixing state on aerosol light absorption and single scattering albedo
35 during air mass aging at a polluted regional site in northeastern China, *Journal of*
36 *Geophysical Research: Atmospheres*, 114, D00G10, 10.1029/2008JD010883, 2009.
- 37 Cheng, Y. F., Su, H., Rose, D., Gunthe, S. S., Berghof, M., Wehner, B., Achtert, P., Nowak, A.,
38 Takegawa, N., Kondo, Y., Shiraiwa, M., Gong, Y. G., Shao, M., Hu, M., Zhu, T., Zhang,
39 Y. H., Carmichael, G. R., Wiedensohler, A., Andreae, M. O., and Pöschl, U.: Size-resolved
40 measurement of the mixing state of soot in the megacity Beijing, China: diurnal cycle,
41 aging and parameterization, *Atmos. Chem. Phys.*, 12, 4477-4491, 10.5194/acp-12-4477-
42 2012, 2012.

- 1 Chow, J. C., Watson, J. G., Lowenthal, D. H., Solomon, P. A., Magliano, K. L., Ziman, S. D.,
2 and Richards, L. W.: PM10 and PM2.5 compositions in California's San Joaquin Valley,
3 *Aerosol Science and Technology*, 18, 105-128, 1993.
- 4 Chow, J. C., Watson, J. G., Lu, Z., Lowenthal, D. H., Frazier, C. A., Solomon, P. A., Thuillier,
5 R. H., and Magliano, K.: Descriptive analysis of PM2.5 and PM10 at regionally
6 representative locations during SJVAQS/AUSPEX, *Atmos. Environ.*, 30, 2079-2112,
7 [http://dx.doi.org/10.1016/1352-2310\(95\)00402-5](http://dx.doi.org/10.1016/1352-2310(95)00402-5), 1996.
- 8 Chow, J. C., Yu, J. Z., Watson, J. G., Hang Ho, S. S., Bohannon, T. L., Hays, M. D., and Fung,
9 K. K.: The application of thermal methods for determining chemical composition of
10 carbonaceous aerosols: A review, *Journal of Environmental Science and Health Part A*, 42,
11 1521-1541, 2007.
- 12 Donahue, N. M., Robinson, A. L., and Pandis, S. N.: Atmospheric organic particulate matter:
13 From smoke to secondary organic aerosol, *Atmospheric Environment*, 43, 94-106,
14 <http://dx.doi.org/10.1016/j.atmosenv.2008.09.055>, 2009.
- 15 Donahue, N. M., Epstein, S. A., Pandis, S. N., and Robinson, A. L.: A two-dimensional
16 volatility basis set: 1. organic-aerosol mixing thermodynamics, *Atmos. Chem. Phys.*, 11,
17 3303-3318, 10.5194/acp-11-3303-2011, 2011.
- 18 Donahue, N. M., Kroll, J. H., Pandis, S. N., and Robinson, A. L.: A two-dimensional volatility
19 basis set – Part 2: Diagnostics of organic-aerosol evolution, *Atmos. Chem. Phys.*, 12, 615-
20 634, 10.5194/acp-12-615-2012, 2012.
- 21 Frey, A., Rose, D., Wehner, B., Müller, T., Cheng, Y., Wiedensohler, A., and Virkkula, A.:
22 Application of the Volatility-TDMA Technique to Determine the Number Size
23 Distribution and Mass Concentration of Less Volatile Particles, *Aerosol Science and
24 Technology*, 42, 817-828, 10.1080/02786820802339595, 2008.
- 25 Fuller, K. A., Malm, W. C., and Kreidenweis, S. M.: Effects of mixing on extinction by
26 carbonaceous particles, *Journal of Geophysical Research: Atmospheres*, 104, 15941-15954,
27 10.1029/1998JD100069, 1999.
- 28 Ghazi, R., and Olfert, J. S.: Coating Mass Dependence of Soot Aggregate Restructuring due to
29 Coatings of Oleic Acid and Dioctyl Sebacate, *Aerosol Science and Technology*, 47, 192-
30 200, 10.1080/02786826.2012.741273, 2012.
- 31 Gnauk, T., Müller, K., van Pinxteren, D., He, L.-Y., Niu, Y., Hu, M., and Herrmann, H.: Size-
32 segregated particulate chemical composition in Xinken, Pearl River Delta, China: OC/EC
33 and organic compounds, *Atmos. Environ.*, 42, 6296-6309,
34 <http://dx.doi.org/10.1016/j.atmosenv.2008.05.001>, 2008.
- 35 Gu, J., Du, S., Han, D., Hou, L., Yi, J., Xu, J., Liu, G., Han, B., Yang, G., and Bai, Z.-P.: Major
36 chemical compositions, possible sources, and mass closure analysis of PM2.5 in Jinan,
37 China, *Air Quality, Atmosphere & Health*, 7, 251-262, 10.1007/s11869-013-0232-9, 2014.
- 38 Häkkinen, S. A. K., Äijälä M., Lehtipalo, K., Junninen, H., Backman, J., Virkkula, A.,
39 Nieminen, T., Vestenius, M., Hakola, H., Ehn, M., Worsnop, D. R., Kulmala, M., Petäjä
40 T., and Riipinen, I.: Long-term volatility measurements of submicron atmospheric aerosol
41 in Hyytiälä Finland, *Atmos. Chem. Phys.*, 12, 10771-10786, 10.5194/acp-12-10771-2012,
42 2012.

- 1 Hansen, A. D. A., Rosen, H., and Novakov, T.: The Aethalometer - An Instrument for the Real-
2 Time Measurement of Optical-Absorption by Aerosol-Particles *Sci. Total Environ.*, 36,
3 191-196, 10.1016/0048-9697(84)90265-1, 1984.
- 4 Hitzenberger, R., Jennings, S. G., Larson, S. M., Dillner, A., Cachier, H., Galambos, Z., Rouc,
5 A., and Spain, T. G.: Intercomparison of measurement methods for black carbon aerosols,
6 *Atmos. Environ.*, 33, 2823-2833, [http://dx.doi.org/10.1016/S1352-2310\(98\)00360-4](http://dx.doi.org/10.1016/S1352-2310(98)00360-4), 1999.
- 7 Horvath, H.: Atmospheric light absorption—A review, *Atmospheric Environment. Part A.*
8 *General Topics*, 27, 293-317, [http://dx.doi.org/10.1016/0960-1686\(93\)90104-7](http://dx.doi.org/10.1016/0960-1686(93)90104-7), 1993.
- 9 Huang, X.-F., Yu, J. Z., He, L.-Y., and Hu, M.: Size Distribution Characteristics of Elemental
10 Carbon Emitted from Chinese Vehicles: Results of a Tunnel Study and Atmospheric
11 Implications, *Environmental Science & Technology*, 40, 5355-5360, 10.1021/es0607281,
12 2006.
- 13 Huffman, J. A., Docherty, K. S., Aiken, A. C., Cubison, M. J., Ulbrich, I. M., DeCarlo, P. F.,
14 Sueper, D., Jayne, J. T., Worsnop, D. R., Ziemann, P. J., and Jimenez, J. L.: Chemically-
15 resolved aerosol volatility measurements from two megacity field studies, *Atmos. Chem.*
16 *Phys.*, 9, 7161-7182, 10.5194/acp-9-7161-2009, 2009.
- 17 Japar, S. M., Brachaczek, W. W., Gorse Jr, R. A., Norbeck, J. M., and Pierson, W. R.: The
18 contribution of elemental carbon to the optical properties of rural atmospheric aerosols,
19 *Atmospheric Environment (1967)*, 20, 1281-1289, [http://dx.doi.org/10.1016/0004-](http://dx.doi.org/10.1016/0004-6981(86)90163-0)
20 [6981\(86\)90163-0](http://dx.doi.org/10.1016/0004-6981(86)90163-0), 1986.
- 21 Kalberer, M., Paulsen, D., Sax, M., Steinbacher, M., Dommen, J., Prevot, A. S. H., Fisseha, R.,
22 Weingartner, E., Frankevich, V., Zenobi, R., and Baltensperger, U.: *Science*, 303, 1659,
23 2004.
- 24 Kirchstetter, T. W., Novakov, T., and Hobbs, P. V.: Evidence that the spectral dependence of
25 light absorption by aerosols is affected by organic carbon, *Journal of Geophysical Research:*
26 *Atmospheres*, 109, D21208, 10.1029/2004JD004999, 2004.
- 27 Kondo, Y., Komazaki, Y., Miyazaki, Y., Moteki, N., Takegawa, N., Kodama, D., Deguchi, S.,
28 Nogami, M., Fukuda, M., Miyakawa, T., Morino, Y., Koike, M., Sakurai, H., and Ehara,
29 K.: Temporal variations of elemental carbon in Tokyo, *Journal of Geophysical Research:*
30 *Atmospheres*, 111, D12205, 10.1029/2005JD006257, 2006.
- 31 Kuwata, M., Kondo, Y., Mochida, M., Takegawa, N., and Kawamura, K.: Dependence of CCN
32 activity of less volatile particles on the amount of coating observed in Tokyo, *Journal of*
33 *Geophysical Research: Atmospheres*, 112, D11207, 10.1029/2006JD007758, 2007.
- 34 Lavanchy, V. M. H., G äggeler, H. W., Nyeki, S., and Baltensperger, U.: Elemental carbon (EC)
35 and black carbon (BC) measurements with a thermal method and an aethalometer at the
36 high-alpine research station Jungfrauoch, *Atmos. Environ.*, 33, 2759-2769,
37 [http://dx.doi.org/10.1016/S1352-2310\(98\)00328-8](http://dx.doi.org/10.1016/S1352-2310(98)00328-8), 1999.
- 38 Lee, B. P., Li, Y. J., Yu, J. Z., Louie, P. K. K., and Chan, C. K.: Physical and chemical
39 characterization of ambient aerosol by HR-ToF-AMS at a suburban site in Hong Kong
40 during springtime 2011, *Journal of Geophysical Research: Atmospheres*, 118, 8625-8639,
41 10.1002/jgrd.50658, 2013.
- 42 Levy, M. E., Zhang, R., Zheng, J., Tan, H., Wang, Y., Molina, L. T., Takahama, S., Russell, L.
43 M., and Li, G.: Measurements of submicron aerosols at the California–Mexico border

- 1 during the Cal–Mex 2010 field campaign, *Atmos. Environ.*, 88, 308-319,
2 <http://dx.doi.org/10.1016/j.atmosenv.2013.08.062>, 2014.
- 3 Liousse, C., Cachier, H., and Jennings, S. G.: Optical and thermal measurements of black
4 carbon aerosol content in different environments: Variation of the specific attenuation
5 cross-section, σ , *Atmospheric Environment. Part A. General Topics*, 27, 1203-
6 1211, [http://dx.doi.org/10.1016/0960-1686\(93\)90246-U](http://dx.doi.org/10.1016/0960-1686(93)90246-U), 1993.
- 7 Lo, J. C. F., Lau, A. K. H., Fung, J. C. H., and Chen, F.: Investigation of enhanced cross-city
8 transport and trapping of air pollutants by coastal and urban land-sea breeze circulations,
9 *Journal of Geophysical Research: Atmospheres*, 111, n/a-n/a, 10.1029/2005JD006837,
10 2006.
- 11 Murphy, B. N., Donahue, N. M., Robinson, A. L., and Pandis, S. N.: A naming convention for
12 atmospheric organic aerosol, *Atmos. Chem. Phys.*, 14, 5825-5839, 10.5194/acp-14-5825-
13 2014, 2014.
- 14 Novakov, T., Ramanathan, V., Hansen, J. E., Kirchstetter, T. W., Sato, M., Sinton, J. E., and
15 Sathaye, J. A.: Large historical changes of fossil-fuel black carbon aerosols, *Geophysical
16 Research Letters*, 30, 4, 10.1029/2002gl016345, 2003.
- 17 Onasch, T. B., Trimborn, A., Fortner, E. C., Jayne, J. T., Kok, G. L., Williams, L. R., Davidovits,
18 P., and Worsnop, D. R.: Soot Particle Aerosol Mass Spectrometer: Development,
19 Validation, and Initial Application, *Aerosol Science and Technology*, 46, 804-817,
20 10.1080/02786826.2012.663948, 2012.
- 21 Penner, J. E., and Novakov, T.: Carbonaceous particles in the atmosphere: A historical
22 perspective to the Fifth International Conference on Carbonaceous Particles in the
23 Atmosphere, *Journal of Geophysical Research: Atmospheres*, 101, 19373-19378,
24 10.1029/96JD01175, 1996.
- 25 Petzold, A., and Schönlinner, M.: Multi-angle absorption photometry—a new method for the
26 measurement of aerosol light absorption and atmospheric black carbon, *Journal of Aerosol
27 Science*, 35, 421-441, <http://dx.doi.org/10.1016/j.jaerosci.2003.09.005>, 2004.
- 28 Philippin, S., Wiedensohler, A., and Stratmann, F.: Measurements of non-volatile fractions of
29 pollution aerosols with an eight-tube volatility tandem differential mobility analyzer
30 (VTDMA-8), *Journal of Aerosol Science*, 35, 185-203,
31 <http://dx.doi.org/10.1016/j.jaerosci.2003.07.004>, 2004.
- 32 Pinnick, R., Jennings, S., and Fernandez, G.: Volatility of aerosols in the arid southwestern
33 United States, *Journal of the atmospheric sciences*, 44, 562-576, 1987.
- 34 Putaud, J. P., Van Dingenen, R., Alastuey, A., Bauer, H., Birmili, W., Cyrus, J., Flentje, H.,
35 Fuzzi, S., Gehrig, R., Hansson, H. C., Harrison, R. M., Herrmann, H., Hitzenberger, R.,
36 Hüglin, C., Jones, A. M., Kasper-Giebl, A., Kiss, G., Kousa, A., Kuhlbusch, T. A. J.,
37 Löschau, G., Maenhaut, W., Molnar, A., Moreno, T., Pekkanen, J., Perrino, C., Pitz, M.,
38 Puxbaum, H., Querol, X., Rodriguez, S., Salma, I., Schwarz, J., Smolik, J., Schneider, J.,
39 Spindler, G., ten Brink, H., Tursic, J., Viana, M., Wiedensohler, A., and Raes, F.: A
40 European aerosol phenomenology – 3: Physical and chemical characteristics of particulate
41 matter from 60 rural, urban, and kerbside sites across Europe, *Atmos. Environ.*, 44, 1308-
42 1320, <http://dx.doi.org/10.1016/j.atmosenv.2009.12.011>, 2010.
- 43 Rader, D. J., and McMurry, P. H.: Application of the tandem differential mobility analyzer to
44 studies of droplet growth or evaporation, *Journal of Aerosol Science*, 17, 771-787, 1986.

- 1 Robinson, A. L., Donahue, N. M., Shrivastava, M. K., Weitkamp, E. A., Sage, A. M., Grieshop,
2 A. P., Lane, T. E., Pierce, J. R., and Pandis, S. N.: Rethinking organic aerosols:
3 Semivolatile emissions and photochemical aging, *Science*, 315, 1259-1262,
4 10.1126/science.1133061, 2007.
- 5 Rolph, G. D.: Real-time Environmental Applications and Display sYstem (READY) Website
6 (<http://www.ready.noaa.gov>), 2016.
- 7 Rose, D., Wehner, B., Ketzel, M., Engler, C., Voigtlander, J., Tuch, T., and Wiedensohler, A.:
8 Atmospheric number size distributions of soot particles and estimation of emission factors,
9 *Atmos. Chem. Phys.*, 6, 1021-1031, 10.5194/acp-6-1021-2006, 2006.
- 10 Rose, D., Gunthe, S. S., Su, H., Garland, R. M., Yang, H., Berghof, M., Cheng, Y. F., Wehner,
11 B., Achtert, P., Nowak, A., Wiedensohler, A., Takegawa, N., Kondo, Y., Hu, M., Zhang,
12 Y., Andreae, M. O., and Pöschl, U.: Cloud condensation nuclei in polluted air and biomass
13 burning smoke near the mega-city Guangzhou, China – Part 2: Size-resolved aerosol
14 chemical composition, diurnal cycles, and externally mixed weakly CCN-active soot
15 particles, *Atmos. Chem. Phys.*, 11, 2817-2836, 10.5194/acp-11-2817-2011, 2011.
- 16 Rosen, H., Hansen, A. D. A., Gundel, L., and Novakov, T.: Identification of the optically
17 absorbing component in urban aerosols, *Applied Optics*, 17, 3859-3861,
18 10.1364/AO.17.003859, 1978.
- 19 Schauer, J. J., Mader, B. T., Deminter, J. T., Heidemann, G., Bae, M. S., Seinfeld, J. H., Flagan,
20 R. C., Cary, R. A., Smith, D., Huebert, B. J., Bertram, T., Howell, S., Kline, J. T., Quinn,
21 P., Bates, T., Turpin, B., Lim, H. J., Yu, J. Z., Yang, H., and Keywood, M. D.: ACE-Asia
22 intercomparison of a thermal-optical method for the determination of particle-phase
23 organic and elemental carbon, *Environmental Science & Technology*, 37, 993-1001,
24 10.1021/es020622f, 2003.
- 25 Stein, A. F., Draxler, R. R., Rolph, G. D., Stunder, B. J. B., Cohen, M. D., and Ngan, F.:
26 NOAA's HYSPLIT Atmospheric Transport and Dispersion Modeling System, *Bulletin of
27 the American Meteorological Society*, 96, 2059-2077, 10.1175/BAMS-D-14-00110.1,
28 2015.
- 29 Stephens, M., Turner, N., and Sandberg, J.: Particle identification by laser-induced
30 incandescence in a solid-state laser cavity, *Applied Optics*, 42, 3726-3736,
31 10.1364/AO.42.003726, 2003.
- 32 Tan, H. B., Yin, Y., Gu, X. S., Li, F., Chan, P. W., Xu, H. B., Deng, X. J., and Wan, Q. L.: An
33 observational study of the hygroscopic properties of aerosols over the Pearl River Delta
34 region, *Atmos. Environ.*, 77, 817-826, 10.1016/j.atmosenv.2013.05.049, 2013a.
- 35 Tan, H. B., Xu, H. B., Wan, Q. L., Li, F., Deng, X. J., Chan, P. W., Xia, D., and Yin, Y.: Design
36 and Application of an Unattended Multifunctional H-TDMA System, *Journal of
37 Atmospheric and Oceanic Technology*, 30, 1136-1148, 10.1175/JTECH-D-12-00129.1,
38 2013b.
- 39 Tao, J., Zhang, L., Ho, K., Zhang, R., Lin, Z., Zhang, Z., Lin, M., Cao, J., Liu, S., and Wang,
40 G.: Impact of PM_{2.5} chemical compositions on aerosol light scattering in Guangzhou —
41 the largest megacity in South China, *Atmospheric Research*, 135–136, 48-58,
42 <http://dx.doi.org/10.1016/j.atmosres.2013.08.015>, 2014.

- 1 Turpin, B. J., Cary, R. A., and Huntzicker, J. J.: An In Situ, Time-Resolved Analyzer for
2 Aerosol Organic and Elemental Carbon, *Aerosol Science and Technology*, 12, 161-171,
3 10.1080/02786829008959336, 1990.
- 4 Twomey, S.: On the composition of cloud nuclei in the northeastern United States, *J. Rech.*
5 *Atmos*, 3, 281-285, 1968.
- 6 Villani, P., Picard, D., Marchand*, N., and Laj, P.: Design and Validation of a 6-Volatility
7 Tandem Differential Mobility Analyzer (VTDMA), *Aerosol Science and Technology*, 41,
8 898-906, 10.1080/02786820701534593, 2007.
- 9 Virkkula, A., Ahlquist, N. C., Covert, D. S., Arnott, W. P., Sheridan, P. J., Quinn, P. K., and
10 Coffman, D. J.: Modification, Calibration and a Field Test of an Instrument for Measuring
11 Light Absorption by Particles, *Aerosol Science and Technology*, 39, 68-83,
12 10.1080/027868290901963, 2005.
- 13 Wehner, B., Philippin, S., Wiedensohler, A., Scheer, V., and Vogt, R.: Variability of non-
14 volatile fractions of atmospheric aerosol particles with traffic influence, *Atmos. Environ.*,
15 38, 6081-6090, <http://dx.doi.org/10.1016/j.atmosenv.2004.08.015>, 2004.
- 16 Wehner, B., Berghof, M., Cheng, Y. F., Achtert, P., Birmili, W., Nowak, A., Wiedensohler, A.,
17 Garland, R. M., Pöschl, U., Hu, M., and Zhu, T.: Mixing state of nonvolatile aerosol
18 particle fractions and comparison with light absorption in the polluted Beijing region,
19 *Journal of Geophysical Research: Atmospheres*, 114, D00G17, 10.1029/2008JD010923,
20 2009.
- 21 Wu, C., Ng, W. M., Huang, J. X., Wu, D., and Yu, J. Z.: Determination of Elemental and
22 Organic Carbon in PM_{2.5} in the Pearl River Delta Region: Inter-Instrument (Sunset vs.
23 DRI Model 2001 Thermal/Optical Carbon Analyzer) and Inter-Protocol Comparisons
24 (IMPROVE vs. ACE-Asia Protocol), *Aerosol Science and Technology*, 46, 610-621,
25 10.1080/02786826.2011.649313, 2012.
- 26 Wu, D., Bi, X. Y., Deng, X. J., Li, F., Tan, H. B., Liao, G. L., and Huang, J.: Effect of
27 atmospheric haze on the deterioration of visibility over the Pearl River Delta, *Acta*
28 *Meteorol. Sin.*, 21, 215-223, 2007.
- 29 Yu, H., Wu, C., Wu, D., and Yu, J. Z.: Size distributions of elemental carbon and its
30 contribution to light extinction in urban and rural locations in the pearl river delta region,
31 China, *Atmos. Chem. Phys.*, 10, 5107-5119, 10.5194/acp-10-5107-2010, 2010.
- 32 Zhang, S. L., Ma, N., Kecorius, S., Wang, P. C., Hu, M., Wang, Z. B., Größ J., Wu, Z. J., and
33 Wiedensohler, A.: Mixing state of atmospheric particles over the North China Plain, *Atmos.*
34 *Environ.*, 125, Part A, 152-164, <http://dx.doi.org/10.1016/j.atmosenv.2015.10.053>, 2016.
- 35 Zhang, Y., Wang, X., Li, G., Yang, W., Huang, Z., Zhang, Z., Huang, X., Deng, W., Liu, T.,
36 Huang, Z., and Zhang, Z.: Emission factors of fine particles, carbonaceous aerosols and
37 traces gases from road vehicles: Recent tests in an urban tunnel in the Pearl River Delta,
38 China, *Atmos. Environ.*, 122, 876-884, <http://dx.doi.org/10.1016/j.atmosenv.2015.08.024>,
39 2015.
- 40
- 41

1 Table 1. Temperature (T) and residence time (RT) protocol of the semi-continuous Sunset
 2 OC/EC analyzer (Wu et al., 2012)

Carbon Fraction	Carrier Gas	T (°C)	RT (s)
OC ₁	He	310	80
OC ₂		475	60
OC ₃		615	60
OC ₄		870	90
EC ₁	He and 2% O ₂	550	45
EC ₂		625	45
EC ₃		700	45
EC ₄		775	45
EC ₅		850	45
EC ₆		870	45

3

4

1 Table 2. Summary of average number and volume fractions in VTDMA measurements at 300 °C.

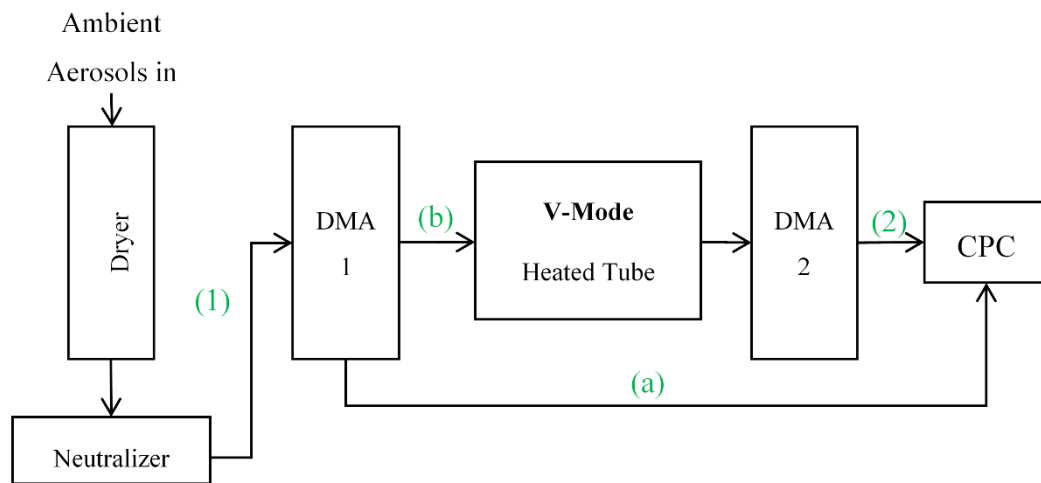
Diameter (nm)	40	80	110	150	200	300
Number fraction						
CV	0.380 ± 0.153	0.174 ± 0.097	0.188 ± 0.081	0.167 ± 0.074	0.153 ± 0.070	0.141 ± 0.065
HV	0.255 ± 0.097	0.198 ± 0.052	0.165 ± 0.055	0.163 ± 0.064	0.178 ± 0.081	0.214 ± 0.097
MV	0.314 ± 0.097	0.513 ± 0.089	0.515 ± 0.098	0.530 ± 0.105	0.523 ± 0.116	0.497 ± 0.125
LV	0.051 ± 0.026	0.113 ± 0.040	0.132 ± 0.041	0.140 ± 0.041	0.146 ± 0.044	0.148 ± 0.047
Volume fraction						
VM	0.503 ± 0.131	0.600 ± 0.082	0.580 ± 0.073	0.590 ± 0.066	0.602 ± 0.064	0.627 ± 0.064
CV	0.361 ± 0.168	0.163 ± 0.105	0.166 ± 0.098	0.148 ± 0.086	0.134 ± 0.080	0.127 ± 0.073
HV	0.014 ± 0.005	0.011 ± 0.003	0.008 ± 0.002	0.007 ± 0.003	0.007 ± 0.003	0.007 ± 0.003
MV	0.070 ± 0.025	0.112 ± 0.024	0.112 ± 0.025	0.115 ± 0.026	0.109 ± 0.027	0.091 ± 0.025
LV	0.052 ± 0.026	0.114 ± 0.040	0.134 ± 0.044	0.140 ± 0.042	0.148 ± 0.048	0.148 ± 0.047

2

1 Table 3. Summary of concentrations of PM_{2.5}, OC, EC and the ratio of OC to EC (OC/EC) in
 2 the five clusters.

	Cluster				
	Coastal	Maritime		Continental	
	1	2	3	4	5
Origin (to the site)	NE	NE/E	NE	NW	NW
PM _{2.5} (µg m ⁻³)	58.5 ± 24.4	58.9 ± 30.9	47.5 ± 28.4	33.9 ± 15.9	33.8 ± 19.3
OC (µg m ⁻³)	10.8 ± 6.01	10.84 ± 7.22	10.13 ± 6.89	5.51 ± 3.3	7.32 ± 2.75
EC (µg m ⁻³)	4.38 ± 2.97	4.98 ± 4.21	3.43 ± 3.12	1.8 ± 0.98	2.46 ± 0.59
OC/EC	2.83 ± 1.05	2.62 ± 1.03	3.65 ± 1.6	3.18 ± 1.26	2.94 ± 0.73

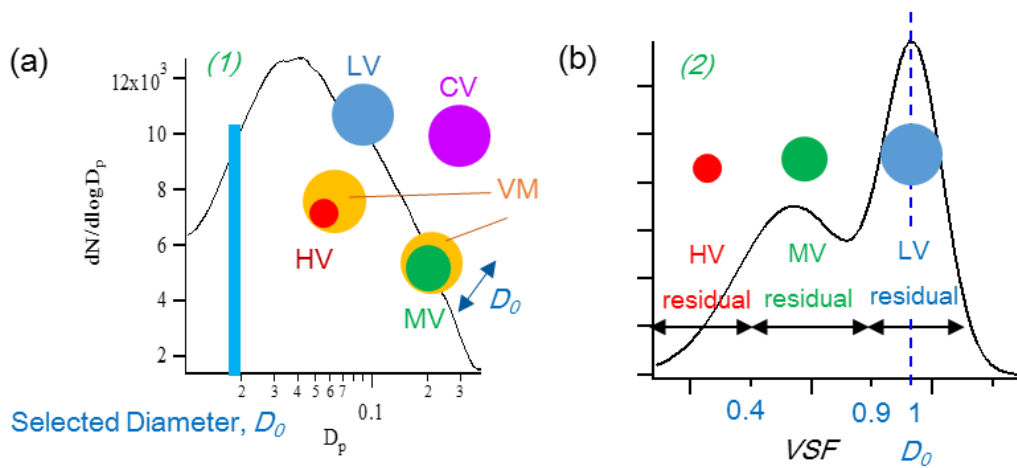
3
 4



1

2 Fig. 1. Schematic diagram of the volatility tandem differential mobility analyzer (VTDMA).

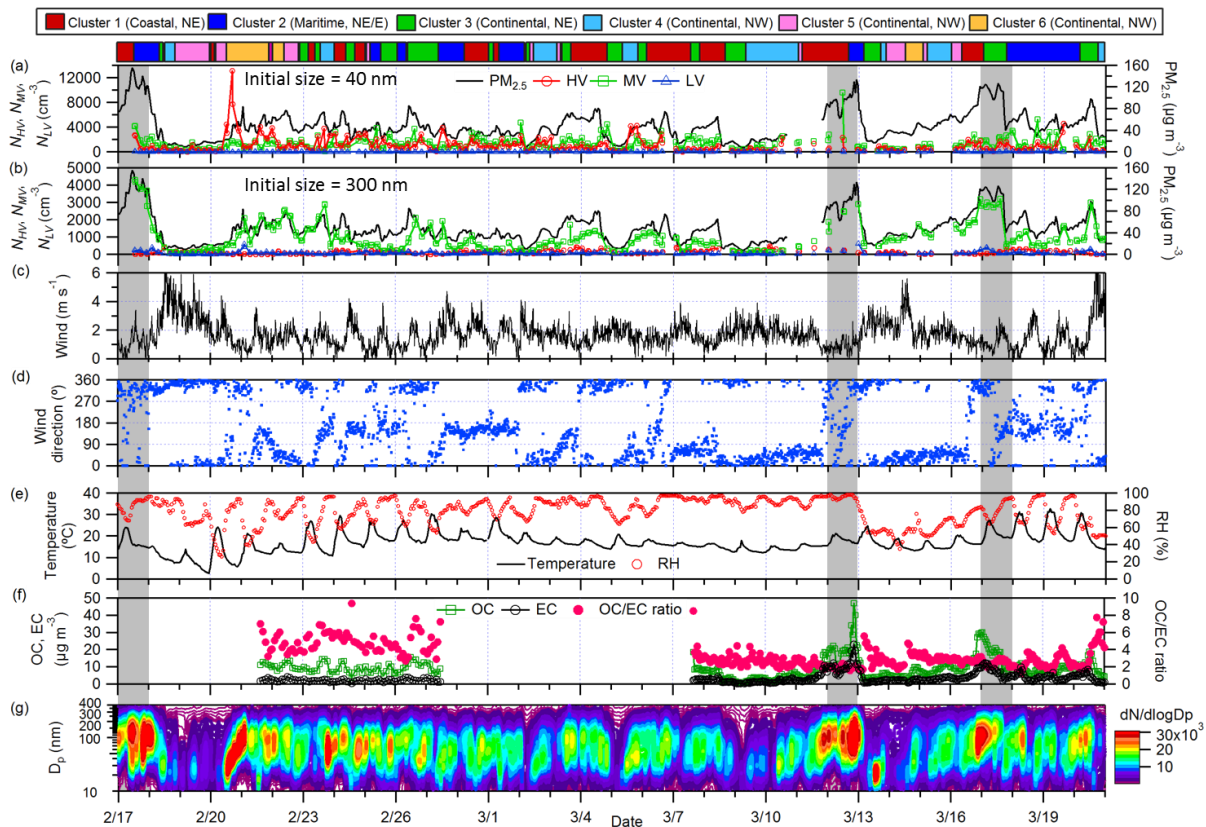
3



1

2 Fig. 2. Examples of particle size distributions of (a) ambient aerosols before entering DMA₁
 3 and (b) residuals of the size-selected particles (D_0) after heating. at 300 °C. The distributions in
 4 Fig. 2a and 2b correspond to (1) and (2) in Figure 1 respectively. Residuals are divided into
 5 three groups—LV (blue), MV (green) and HV (red)—based on their *VSF*. CV (purple) and VM
 6 (orange) are vaporized and hence not measured as residuals. VM appears as coating for
 7 illustration purposes only. It does not necessarily reflect the morphology of the particles.

8



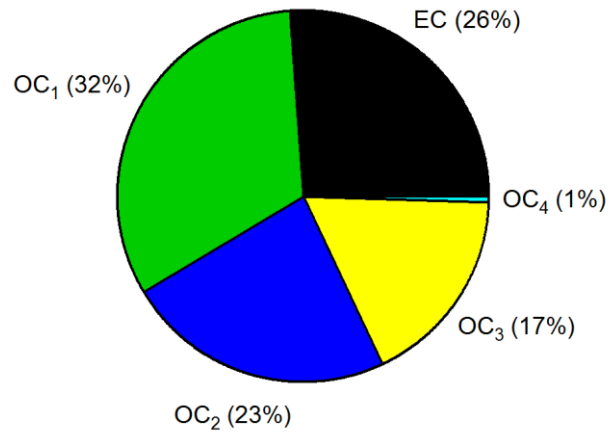
1

2 Fig. 3. Temporal variation of number concentrations of HV, MV and LV in 40 nm
 3 particles, $PM_{2.5}$, major meteorological parameters, OC and EC concentrations, OC-to-EC ratio
 4 and particle number size distributions in the campaign. Air mass clusters are depicted at the top
 5 and the shaded areas indicate days with daily-averaged $PM_{2.5}$ concentrations exceeding $95 \mu g$
 6 m^{-3} .

7

8

9



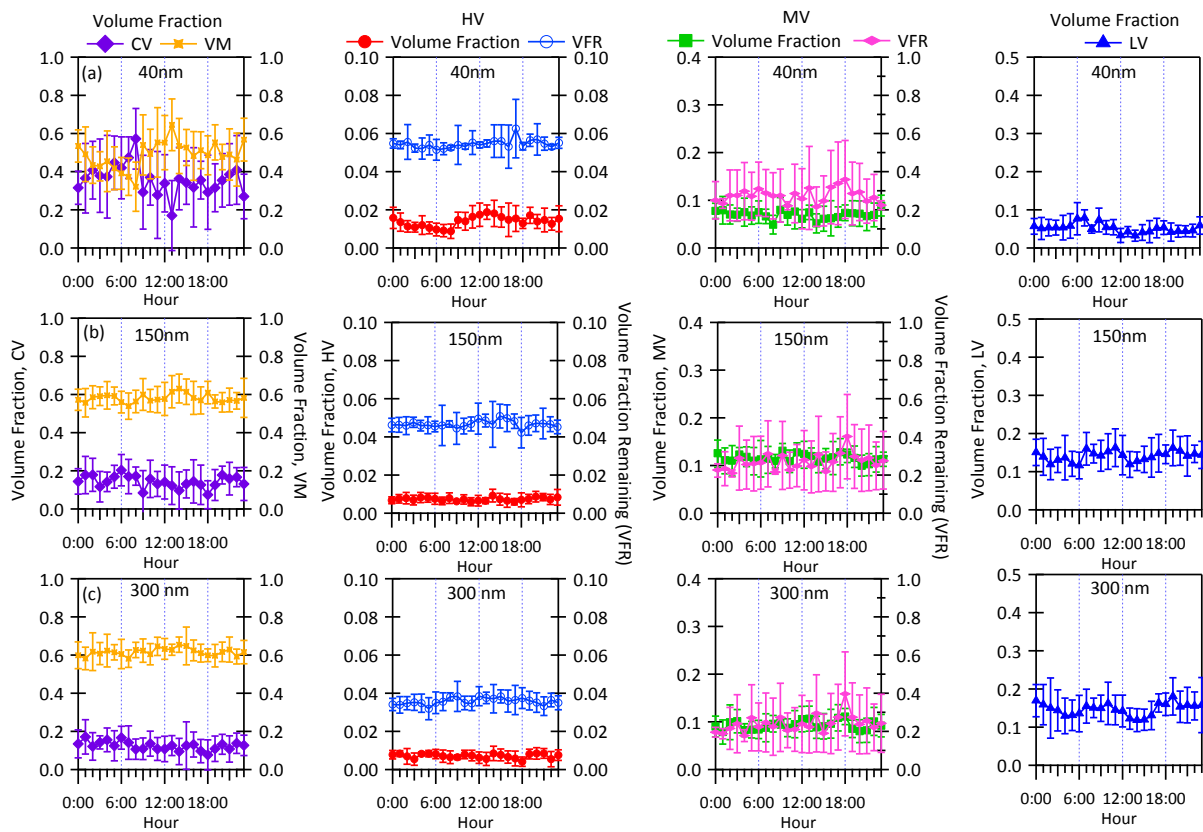
1

2 Fig. 4. Average mass fractions of EC, OC₁, OC₂, OC₃ and OC₄ in PM_{2.5}.

3

4

5

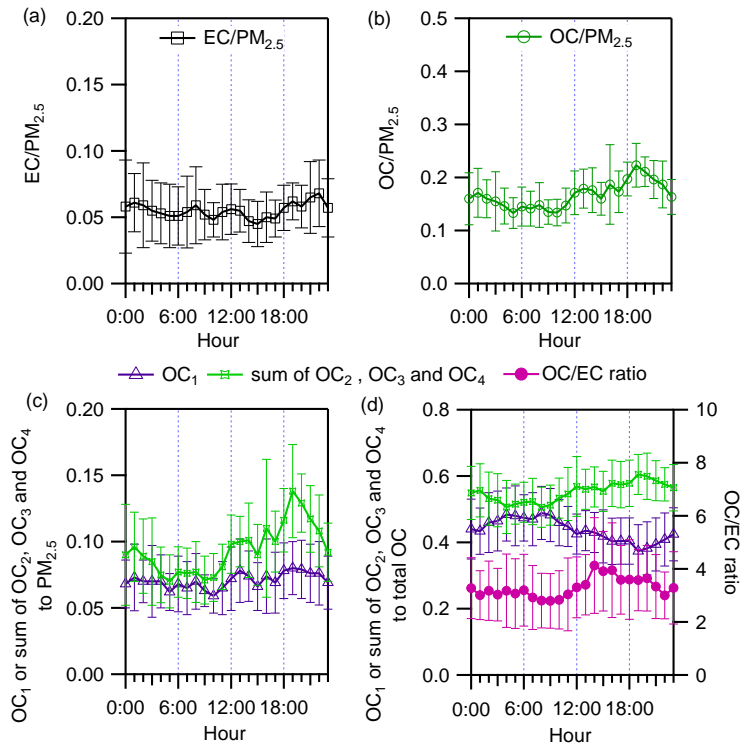


1

2 Fig. 5. Diurnal variations in volume fractions of (columns from left to right) CV, VM, HV
 3 residuals, MV residuals and LV residuals in (a) 40 nm, (b) 150 nm and (c) 300 nm particles.
 4 Diurnal variations in the volume fraction remaining (VFR) of HV and MV particles are plotted
 5 on the right axis. Error bars represent one standard deviation.

6

7

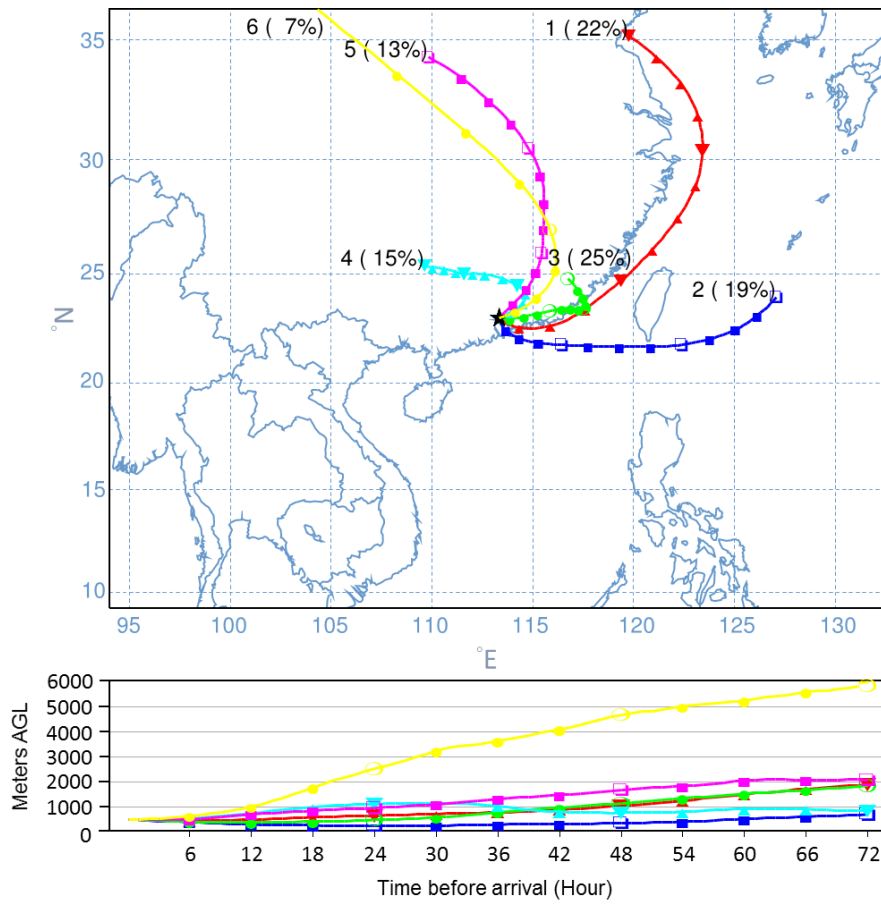


1

2 Fig. 6. Diurnal variations in the mass fractions of EC, OC, OC₁ and the sum of OC₂, OC₃ and
 3 OC₄ in PM_{2.5}, the ratio of OC to EC, mass fractions of OC₁ and the sum of OC₂, OC₃ and OC₄
 4 to total OC in February and March. Error bars represent one standard deviation.

5

6



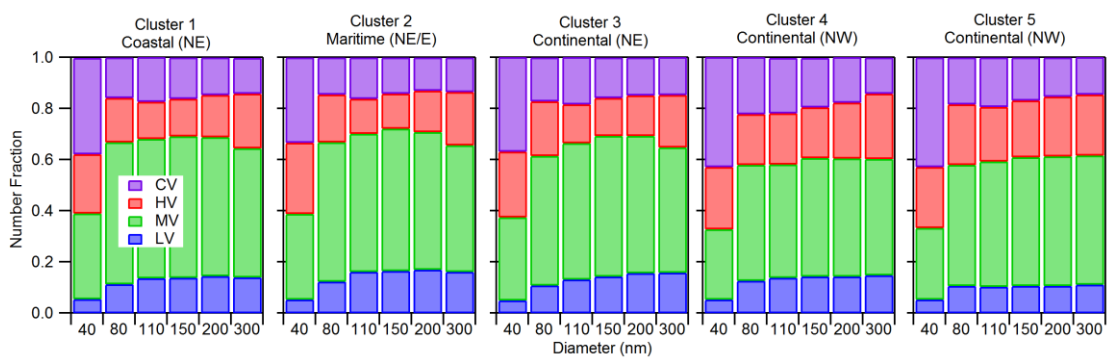
1

2 Fig. 7. Mean back trajectories of the six types of air masses arriving at the sampling site.

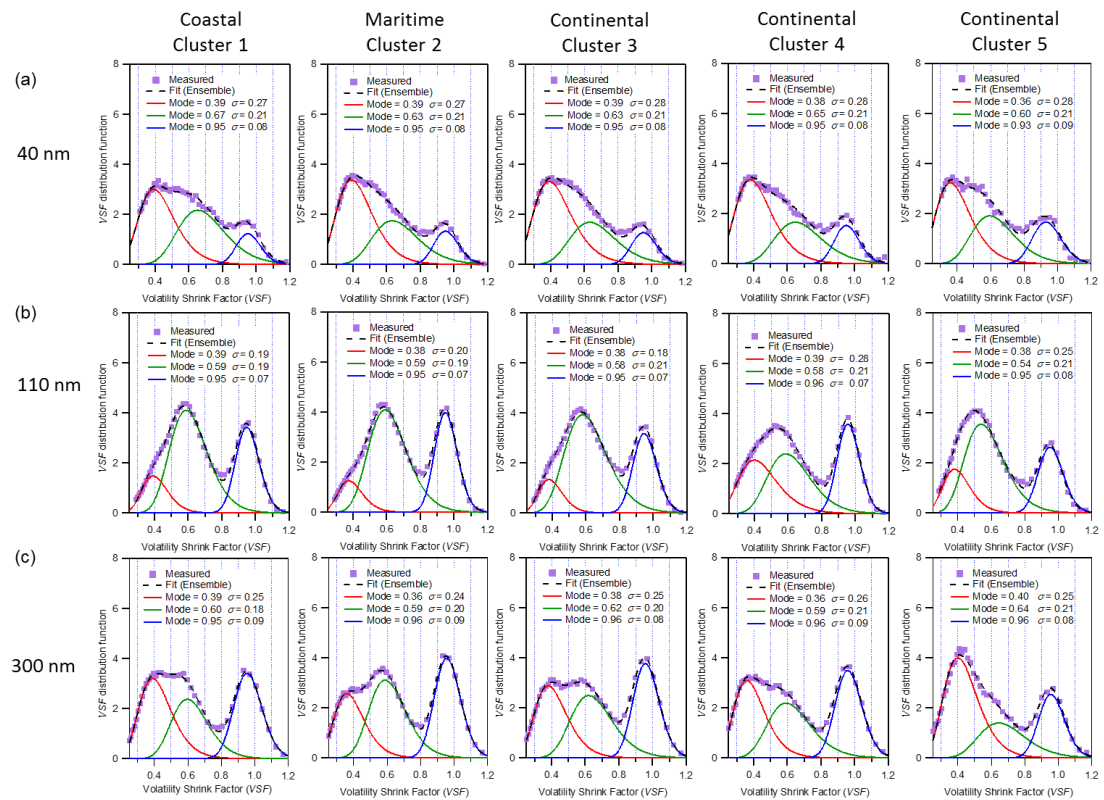
3

4

5

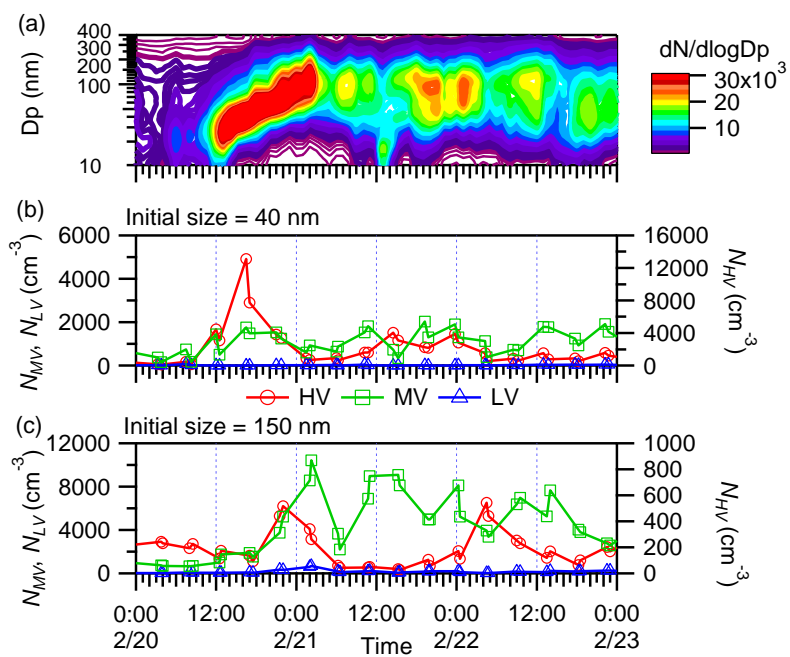


1
 2 Fig. 8. Average number fractions of CV, HV, MV and LV in clusters 1 to 5 at different selected
 3 diameters.
 4



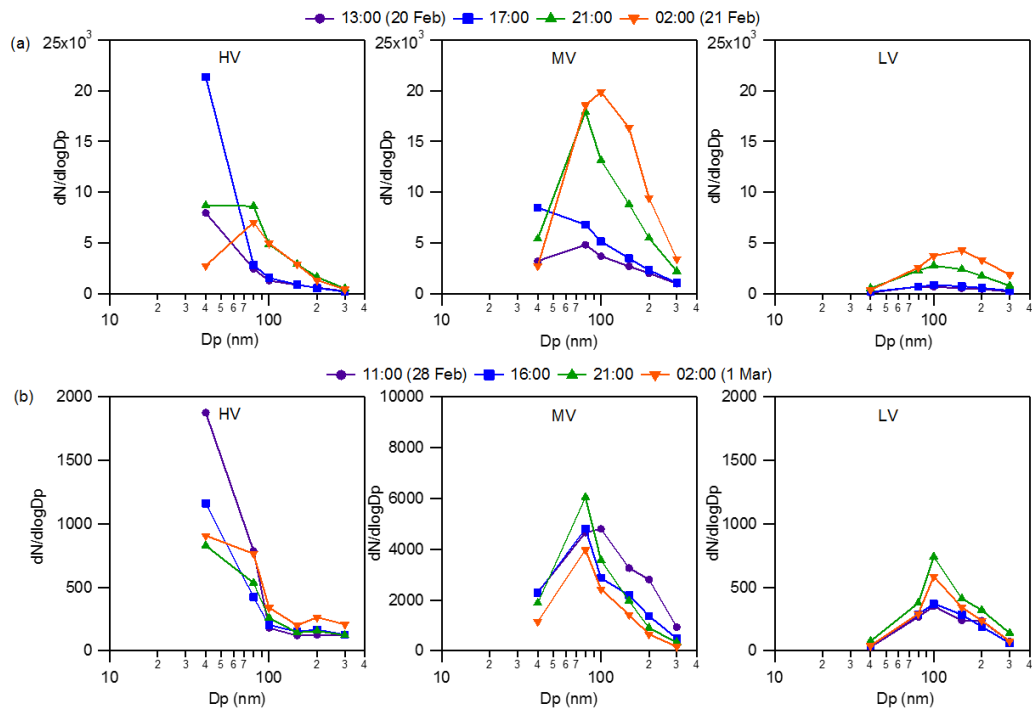
1
2
3
4
5

Fig. 9. Volatility shrinkage factor (*VSF*) distribution function in different clusters. Solid and dotted lines are the peaks fitted with log-normal function and the ensemble distributions, respectively.



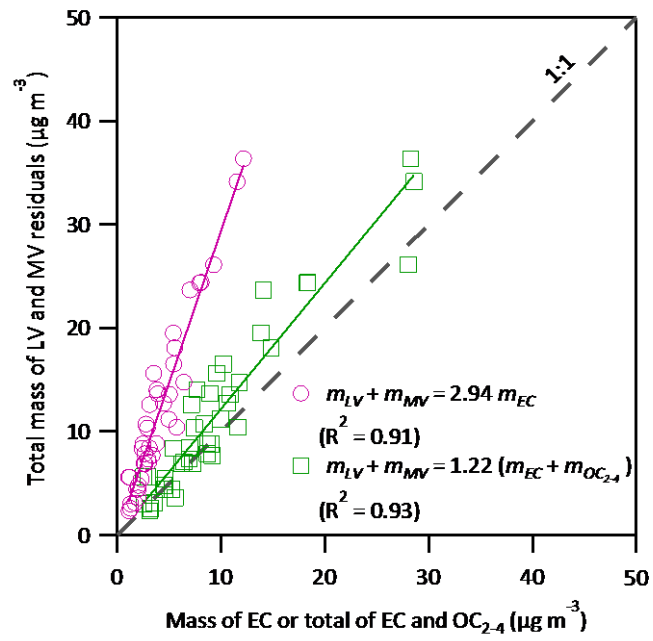
1
 2 Fig. 10. Time series of (a) particle number size distribution, (b) number concentrations of HV,
 3 MV and LV in 40 nm particles and (c) number concentrations of HV, MV and LV in 150 nm
 4 particles.

5



1
 2 Fig. 11. Particle number size distribution of (columns from left to right) HV, MV and LV
 3 particles (a) at 13:00, 17:00, 21:00 on 20 Feb and 02:00 on 21 Feb and (b) at 11:00, 16:00,
 4 21:00 on 28 Feb and 02:00 on 1 Mar.

5
 6
 7



1
2
3
4

Fig. 12. Closure analysis of the total mass of LV and MV residuals from VTDMA at 300 °C and measured mass of EC or total of EC and OC_{2.4} from the OC/EC analyzer.